Desalination and Water Treatment
www.deswater.com

doi: 10.5004/dwt.2018.22288

115 (2018) 236–248
May

Application of surfactant-modified montmorillonitefor As(III) removal from aqueous solutions: kinetics and isotherm study

Samira Soleimani[a], Ghasem Azarian[b], Faramarz Moattar[c], Abdolreza Karbassi[d], Kazem Godini[b,*], Ehsan Niknam[e]

[a]*Department of Environmental health, Faculty of Health, Ilam University of Medical Sciences, Ilam, Iran, email: s.solymani87@gmail.com (S. Soleimani)*
[b]*Department of Environmental Health Engineering, Faculty of Health and Research Center for Health Sciences, Hamadan University of Medical Sciences, Hamadan 65178-38736, Iran, email: gh_azarian@yahoo.com (G. Azarian), Tel. +98 8118381641, Fax +98 8118381641, email: kgoodini@razi.tums.ac.ir (K. Godini)*
[c]*Department of Environmental Science, Graduate School of the Environment and Energy, Science and Research Branch, Islamic Azad University /or Radio-isotope Division, Iran Atomic Energy Organization, Tehran, Iran, email: famoattar@yahoo.com (F. Moattar)*
[d]*Graduate Faculty of Environment, University of Tehran, P.O. Box 12155-6135, Tehran, Iran, email: arkarbassi738@yahoo.com (A. Karbassi)*
[e]*Department of Environmental engineering, Khuzestan Science and Research Branch, Islamic Azad University, Ahvaz, Iran, email: eniknam67@gmail.com (E. Niknam)*

Received 10 January 2017; Accepted 4 April 2018

ABSTRACT

The prime objective of this research was to develop a systematic method for the removal of arsenic (III) from aqueous solutions by adsorption. Thus, montmorillonite modified with tetradecyltrimethylammonium bromide (TTAB) was utilized to prepare an outstanding sorbent. Subsequently, this novel material was characterized and identified completely by different techniques: X-fluorescence spectrometer (XRF), Sear's procedure (titratin method), scanning electron microscopy (SEM), X-ray diffraction (XRD) and Fourier transform infrared spectroscopy (FTIR). Moreover, the effects of solution pH (4–12), surfactant loading rates (20– 200% cation exchange capacity (CEC) of the clay), contact time (10 min–5 h), pollutant concentration (500–3000 µg/l), temperature (15–45 °C) and adsorbent dose (0.1–1.0 g) on the adsorption process were investigated. At the optimum values, the effects of contact time on adsorption and the dependency of adsorption data to different kinetic models like pseudo-first-order, pseudo-second-order, Elovich and intra-particle diffusion were assessed; it was found that the process of arsenic (III) removal followed a pseudo second-order kinetic model ($R^2 = 0.9998$). Following the optimization of the variables, by fitting the experimental equilibrium to the Langmuir, Freundlich, Temkin and Dubinin-Radushkevich models and the respective information for each model and their applicability were examined to understand the conceptual of the adsorption. According to R^2 (0.9999) and maximum adsorption capacity (1.48 mg g^{-1}), it was found that the adsorption process followed the Langmuir model. The thermodynamic study also showed the spontaneous and endothermic nature of the adsorption process.

Keywords: Arsenic (III) adsorption; Surfactant-modified montmorillonite; İsotherm models; Variable optimization

1. Introduction

Arsenic (As), as an environmental toxin, can enter the food chain via both drinking water and crop irrigation [1]. It is an omnipresent trace metalloid and found in nearly all environmental solutions [2]. Long-term As exposure even to very low contents may have dangerous effects [3]: lung, liver, kidney, and bladder cancers, as well as various kinds of skin lesions [4]. As(V) and As(III) are the most common forms of As in natural waters [5]. It should be noted that the

*Corresponding author.

1944-3994 / 1944-3986 © 2018 Desalination Publications. All rights reserved.

treatment of As(III)-laden waters and ground waters is more difficult and its toxicity is by far higher than As(V) [6]. Naturally, more levels of arsenite are present in ground waters, which are more used as drinking water. Nonetheless, the literature review revealed that few studies have been done on arsenite removal from water. In addition, the treatment of water containing As has been attracting the ever-growing attention because of increased strict standards of As in drinking water [7]. Coagulation/precipitation [4], adsorption, membrane separation, ion exchange, bioremediation and so forth have been applied for As(III) removal [8–10]; among these, adsorption, owing to its high removal efficiency, easy operation and low cost and sludge-free properties, has been the most widely employed [11]. Further, it has been known as one of the most important processes controlling As mobility [3]. In water treatment by means of adsorption, it is necessary that inexpensive adsorbents having high adsorption capacities be applied [12].

Various adsorbents like activated carbon [13], activated alumina, hydrous zirconium oxide [14], chitosan [15], hematite [16], magnetite [17], goethite, dolomite [18] have been utilized [19] for the removal of As(III); natural clays are usually regarded as low cost adsorbents, which can remove specific contaminants [20]. In addition, large specific surface area, chemical and mechanical stability, layered structure, and high cation exchange capacity make these adsorbents excellent materials [21]. Although clays have the negative surface charge, they have a weak affinity for heavy metal ions like Co^{2+}, Zn^{2+}, and Cu^{2+}. So as to enhance the sorption ability, surfactants, which are managed by acid or ion exchange, are applied to change swelling clays' surface characteristics [22].

Previous studies have illustrated that Fe and Al oxides and hydroxides have a high affinity to As [23]. Montmorillonite clay (MC) is a typical 2:1 phyllosilicate in which the negative layer charge is electrically balanced by the equal charge of exchangeable cations like Na, Ca, or K [24]. MC contains various exchangeable cations on its surface; the cationic surfactants are widely applied as modifiers. They are used to equilibrate negative charge; organic matters are trapped in the internal layers of soil and increase their distance without creating structural changes in soil matrix and texture and, in turn, adsorptive characteristics of the soil are enhanced.

Many researchers have claimed that the surfactant-modified clays show higher adsorption capacity than the original one [25]. The organoclays are prepared by exchanging Na^{+} or Ca^{2+} cations with cationic surfactants participated on clays' surfaces, where charge on the clay surface is reversed from negative to positive [26]. It has been reported that intercalation of cationic surfactants both changes the surface characteristics of clay from hydrophilic to hydrophobic and raises dramatically the basal spacing of the clay interlayers [27]. This change is as a result of the hydrophobic property of functional groups in surfactants, particularly those with ammonium functional groups, which are not hydrated by water. Many researchers have studied As(III) adsorption by means of clays [27,28]. However, the application of MC modified with cationic surfactants, as an adsorbent in order to remove As from aqueous environments, has been utilized in very few studies [29]. The present study focused on the feasibility of applying montmorillonite modified with tetradecyltrimethylammonium bromide (TTAB) as a low-cost adsorbent for As removal from aqueous media. To our best knowledge, no study has been done in which this surfactant has been used as a soil modifier for As(III) adsorption. The effects of cogeneration of surfactant, pH solution, solute concentration and adsorbent dose on As(III) adsorption onto tetradecyltrimethylammonium bromide montmorillonite clay (T-MC) were studied. Moreover, adsorption kinetics and isotherms parameters were evaluated.

2. Materials and methods

2. 1. Materials and instrumentation

All chemicals: NaOH, KCl, HCl (37%), As_2O_3 and other reagents with the highest purity were purchased from Merck (Darmstadt Germany). The raw MC (98% purity), utilized as the adsorbent, was obtained from Laviosa Co. (Italy). The stock solution (100 mg/L) of As(III) was prepared by dissolving As_2O_3 in distilled water and the working solutions were prepared by successive dilutions of the stock solution. The determination of the specific area of the clay was performed via Sears' method through mixing the MC and T-MC (0.1 g) with 50 ml of 0.1 M HCl solution in a bottle on a magnetic stirrer separately. Sodium chloride salt (10.0 g) was then added to it. The compound was titrated with standard 0.1 M NaOH solution in a water bath at 298±0.5 k, and measured the volume of NaOH solution required to increase the solution pH from 4.0 to 9.0 [30]. The specific areas of the MC and T-MC were calculated using the following equation:

$$S = 32V - 25 \quad (1)$$

where, S (m^2/g) is the surface area of the adsorbent and V (ml) is the volume of spent NaOH solution. In order to identify the structure and morphology of the raw MC and T-MC, Scanning electron microscope (Seron, AIS-2100, South Korea) was applied. X-ray Fluorescence (XRF) data were collected on a PAN alytical Co., MiniPal 4 XRF Spectrometer. A FTIR spectrophotometer (JASCO, FT/IR-6300, Japan) was employed to perform the FTIR analysis of the adsorbent in the range of 400–4000 cm^{-1}. X-ray diffraction (XRD) analysis of the MC and T-MC was determined with an X-ray diffract meter (Bruker, D8ADVANCE, Germany) using Ni filtered Cu Kα radiation (1.5406 Å) at room temperature. And, concentrations were measured by a PerkinElmer (Waltham, MA) AAnalyst 800 graphite furnace atomic absorption spectrometer.

2.2. Clay adsorbent

The cation exchange capacity (CEC) was 86 meq/100 g by means of the ammonium acetate method [31]. Since the natural MC contains many impurities like calcite, quartz and cristobalite [32], thus, MC was purified before the application. The purification was conducted via dissolving 50 g of MC in 1 L of distilled water. The prepared suspension was shaken at 25°C and 250 rpm for 24 h; then, it was centrifuged at 500 rpm for 40 min until the separation of

clay fraction was acquired. This work was caused impurity like iron oxide and quartz to precipitate at the bottom of the centrifuge tubes, due to their higher density. Finally, the solid was dried at 60 °C for 24 h in a drying oven and then crushed and sieved to reach the particle size of 125 µm.

2.3. Modification of adsorbent

TTAB, the surfactant used in this research, was purchased from the Aldrich Chemical Co., (USA). In order to investigate the influence of the sorbed surfactant on the As removal from water, the clay was modified through adding 5 g of MC to the amounts of 0.363, 0.908, 1.272, 1.817, 2.726, 3.634 g of TTAB equal to 20, 50, 70, 100, 150, and 200% CEC of MC that were dissolved in 100 ml of distilled water separately. The dispersions were shaken at 250 rpm and room temperature for 24 h on a rotary shaker. The T-MC was separated by centrifugation, the supernatant was removed, and the solid washed with distilled water. Next, the obtained precipitates were dried at 60 °C for 24 h, ground and sieved to reach the particle size of 125 µm.

2.4. Experiments of As(III) adsorption

The sorption of As(III) on T-MC was surveyed via a separate batch technique, which was carried out by mixing the adsorbent with fixed volume of As(III) solution. The runs, except the one for temperature, were conducted at room temperature (25 °C) in 200-ml glass conical flasks, and agitated by using a shaker machine at 250 rpm. The solution to solid ratio in all experiments was 200:1 (0.50 g of the adsorbent in 100 ml of the As solution). After the mixing period to measure the As(III) concentrations using atomic absorption spectrometer, the aqueous samples in bottles were drawn off and centrifuged at 5000 rpm for 15 min and filtered using whatman filter paper. In the present study, the experiment proceeded following the steps outlined respectively: the impacts of parameters like surfactant loading rates (0.2–2 CEC of the clay), contact time (10 min and 5 h), pollutant concentration (100–3000 µg/l), adsorbent dose (0.1–1.0 g) and temperature (15–45 °C). The adsorption equilibrium isotherm experiments were determined by mixing 0.1 g of the adsorbent with 100 ml of the As(III) solution for a range of As content from 500 to 3000 µg/L at pH 6.0±0.1. The As amount uptake q_e (mg/g) was calculated by the following equation:

$$q_e = \frac{(C_o - C_e)V}{m} \quad (2)$$

where q_e is the capacity of the adsorbent for the pollutant (mg/l), C_o and C_e are the concentrations of initial and final pollutant concentration (mg/l), respectively, V is the volume of the solution (l) and m (g) is the mass of the adsorbent. The amount of As removal was calculated by means of the following equation:

$$R = \frac{C_0 - C_t}{C_0} \times 100 \quad (3)$$

where C_0 (mg·L^{-1}) and C_t (mg·L^{-1}) are the concentrations of target at initial and after time t, respectively.

3. Results and discussion

3.1. Characterization

3.1.1. XRF

The chemical compositions and physiochemical properties of the adsorbent were measured by an X-fluorescence spectrometer and the findings have been given in Table 1. The results illustrated that SiO_2 and Al_2O_3 are the major components of the clay and MgO, Na_2O_3, Fe_2O_3 and CaO are the second highest components (below 5.0 wt%), respectively, and other oxides are present in much smaller amounts (below 1.0 wt%) (35). Silica to alumina ratio (Si/Al) of 2.95 was attained for the MC. The findings of the XRF analysis showed that the wt% of these metals taken in this study accords with that of a similar work. Moreover, the MC had minor impurities of quartz and feldspar [32]. Silica and alumina ratio (Si/Al) of 2.95 was attained for the used adsorbent that was more than the theoretical Si/Al value [21].

3.1.2. Sear's procedure

The properties of a porous material can be explained well by its surface area, which is one of the most useful micro structural parameters. It is the total internal boundary between the solid phase and the pore system [30]. It is measured by sear's procedure (titratin method), which were 32.6 and 26.2 m^2/g, respectively, for MC and T-MC. However, the surface area of the clay become smaller after the modification; it is not surprising because the surfactant cations introduced to the CM occupy the pores otherwise available for ion exchange [33]. These results accord with those of the studies by Krishna et al. [30] and Lucy et al. [33], who suggested that the modification declined specific surface areas.

Table 1
Physicochemical properties of the adsorbent (MC)

Chemical composition	(wt %)
SiO_2	60
Al_2O_3	20.03
Fe_2O_3	2.31
NaO_2	3.02
MgO	4.02
P_2O_5	0.05
K_2O	0.13
CaO	1.46
TiO_2	0.23
MnO	0.03
H_2O	8.71
Mineralogical analysis	%
Montmorillonite	98
Feldspar	0.5-1
Quartz	0.5-1
Other	
CEC (meq/100g)	108
Limit of ignition (%)	7.03

3.1.3. XRD

The modification of the montmorillonite by cation exchange reaction (cationic surfactants) increases the interlayer space because the surfactant enters the layers (38). The XRD patterns for the MC and T-MC have been shown in Fig. 1. The basal spacing of the MC was 12.10 Å and it increased to 18.59 Å after the modification. Changes in the basal space of the modified MC can be interpreted as the intercalation of organic surfactants into the MC interlayer space [34]. This showed the successful formation of the intercalated MC with the surfactant modification. Wang et al. showed a typical diffraction peak of purified surfactant-modified montmorillonites (MMT) is 6.94°, responding to a basal spacing of 12.74A˚. After intercalation with cetyltrimethylammonium bromide (CTAB), this peak disappears. The movement of the typical diffraction peak of MMT to lower angle (5.94°), responding to a basal spacing of 14.89A˚, which indicates the formation of the intercalated nanostructure with the amount of CTAB of 0.5 CEC of MMT [25].

3.1.4. FTIR spectroscopy

The FTIR spectra patterns of the adsorbent before and after the modification have been shown in Fig. 2. MC displays a typical infrared spectroscopic pattern because of the internal vibrations of TO4/2 (T = Si or Al) tetrahedron, which is the primary unit of the structure and is not sensitive to other structural vibrations. The structural stability of these samples is clearly indicated by the appearance of the major peaks at almost the same position in both the modified and unmodified MC [35]. A strong broad band at 1037 cm^{-1} can be attributed to the stretching vibration of the Si–O. It can be seen that both the samples have the characteristic absorption bands of Al-O-Si (at 527 cm^{-1}) and Si–O–Si (at 468 cm^{-1}) [27]. The bands in the region of 2800–3000 cm^{-1} are assigned to the C-H groups showing surfactant loading on MC [35]. By contrast, the absorption band at 3627 cm^{-1}, corresponding to $^{-}$OH stretching vibration of H_2O of MC, weakened and shifted to the lower wave number [25]. This fact indicates that the H_2O content is reduced with the replacement of the hydrated cation by surfactant ions, leading to the surface properties of the MC changing from hydrophilic to hydrophobic [27].

3.1.5. SEM

As shown in Fig. 3a, the scanning electron microscopy (SEM) micrograph of MC indicates rough surface structure, while T-MC is homogenous and smooth. The SEM analysis illustrated that there were holes and cave type openings on the surface of the adsorbent that provide more surface area available for adsorption [36]. The particle surface becomes much smoother than that of the original particle following As(III) adsorption. It can be towing to occupation of pores by surfactant molecules.

3.2. Batch sorption experiments

3.2.1. Effect of surfactant amount

The results of surfactants loading on As(III) adsorption have been presented in Fig. 4. It was found that the adsorption capacity increased with increasing initial surfactant concentration in solution (20–50% CEC) and rapidly decreased by increasing surfactant load up to 70% CEC. Decreasing the adsorption capacity then slowly continued with the loading amount of surfactant until 200% CEC. The observation can be explained that the amount of the surfactant intercalated into the MC galleries increases with an increase in TTAB, which results in an increase in As(III) absorption [25]. Jiang et al. suggested that the phenol adsorption capacity increased with increasing (Hexdecyl-trimethyl-ammonium bromide, HDTMA) surfactant ratio to 0.2 mmol/g [37] while Li Wang et al. claimed that the adsorption capacities of CTAB-MMT boosted with increasing the contents of CTAB (2.0 CEC) [25]. The higher surfactant loading rates, beyond 70% CEC, may lead to complete occupancy of the interior pores of the adsorbent preventing As(III) being adsorbed. The T-MC with surfactant loading rate of 70% CEC was selected for the subsequent experiments in this study.

3.2.2. Effect of contact time

Equilibrium time is one of the major factors to design a low cost adsorption processes. In the present study, the adsorption of As(III) onto the T-MC at various initial contents was studied as a function of contact time to determine the necessary adsorption equilibrium time. The impact of

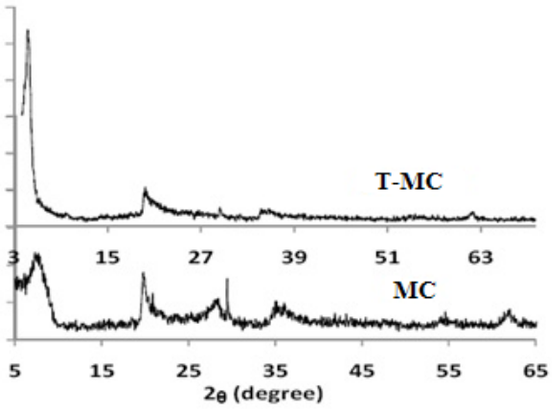

Fig. 1. XRD analysis of MC and T-MC.

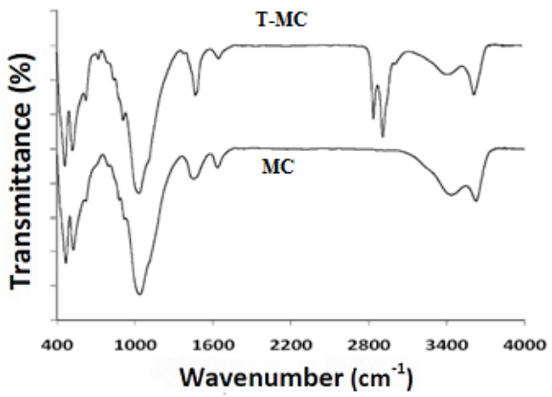

Fig. 2. FTIR analysis of MC and T-MC.

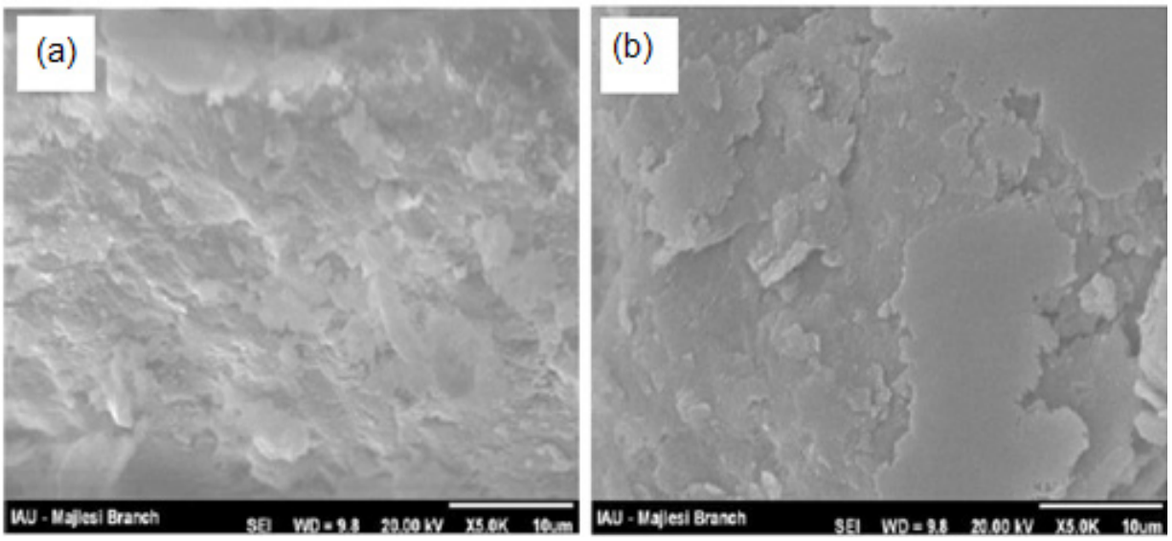

Fig. 3. The SEM micrograph of (a) MC, and (b) T-MC.

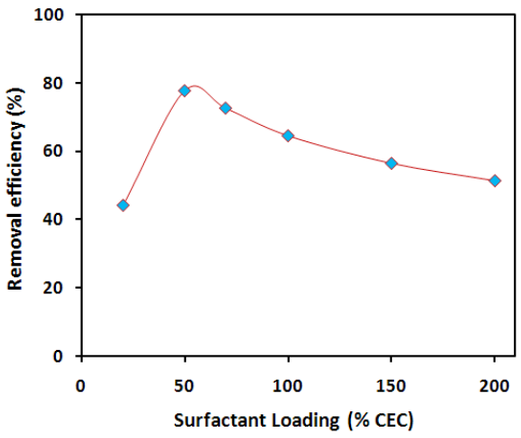

Fig. 4. Effect of surfactants loading on As(III) adsorption onto T-MC: As(III) concentration 1.5 mg/L, initial pH 7.0, contact time 300 min and adsorbent dose 0.5 g/L.

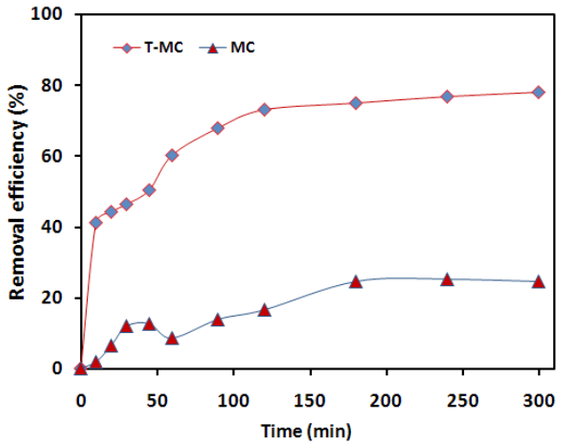

Fig. 5. Effect of contact time on As(III) adsorption by T-MC: As(III) concentration 1.5 mg/L, initial pH 7.0 and adsorbent dose 0.5 g/L.

content on adsorption of As(III) was surveyed to describe As(III) removal rate. Removal efficiency of As(III) by T-MC and MC against contact time is presented in Fig. 5. This figure shows that, although removal efficiency of the raw montmorillonite is low, its modification with a surfactant can increase its performance. The curves in this figure show the quick As(III) adsorption in the very beginning, which may be on account of the relative large numbers of available vacant sites on the T-MC surface as compared to the later contact times [38]. The amount of adsorption was high during the first 2 h, but, after this time, it decreased somewhat, which is because of intra-particle diffusion. The higher adsorption was obtained at 300 min of contact time. Xiaomin Dou et al. stated that the rate of As uptake on schwertmannite adsorbents was fast and 40–50% of the total adsorption occurred within the 2 h of contact time [39]. Thus, the uptake of As(III) by T-MC is dependent upon time. Therefore, the contact time of 5 h was selected for the experiments.

3.2.3. Effect of pH

The pH variable highly affects the ability of adsorbent surface for interaction and metal ion tendency for binding to solid surface. Obviously, this is owing to the effect of pH on the surface properties of an adsorbent and ionization/dissociation of the adsorbate molecule. This variable profoundly influences the metal ion adsorption. It affects both the surface properties of an adsorbent and the speciation of the metal ion in solution [28]. The adsorption capacity of As(III) at different pH values [4,5,40] has been presented in Fig. 6. Under acidic conditions (pH 4.0–5.0), As adsorption

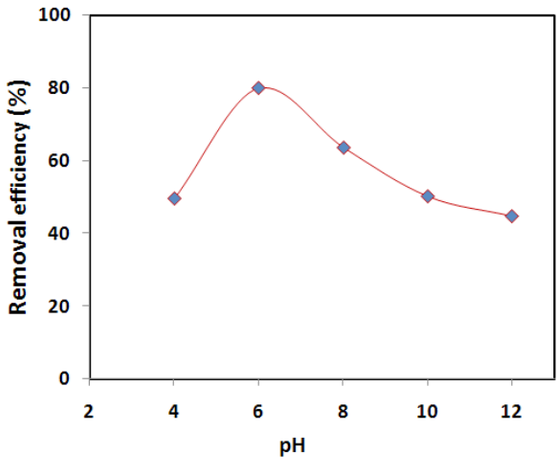

Fig. 6. Effect of pH on As(III) adsorption onto T-MC: As(III) concentration 1.5 mg/L, contact time 300 min and adsorbent dose 0.5 g/L.

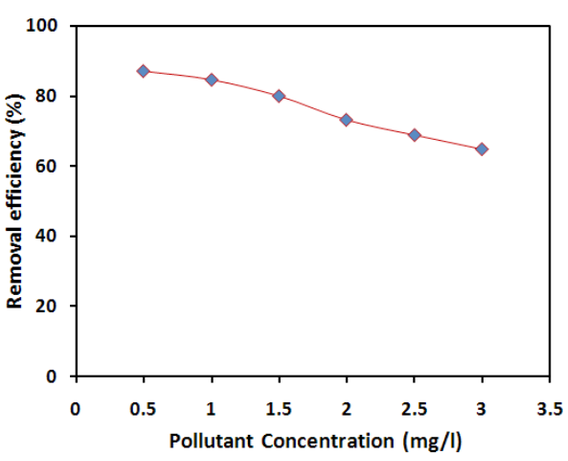

Fig. 7. Effect of pollutant concentration on As(III) adsorption onto T-MC: initial pH 6.0, contact time 300 min and adsorbent dose 0.5 g/L.

by means of the T-MC improved and reached a maximum at pH 6. Similar findings were reported by L.M Camacho et al., who studied As adsorption by clinoptilolite zeolite [33]. Also, Xiaofei Sun et al. suggested that As(III) removal is a highly pH-dependent process as the highest amount of adsorption happened under acidic conditions, and it decreased with increasing solution pH. The decrease in the adsorption yields at pH over 7, which can be because of the higher negative charge of As(III) species and the negative charge of the adsorbent [41].

3.2.4. Effect of pollutant concentration

It has been proved that the removal amount of adsorption is dependent on the ratio of the number of adsorbate moiety to the available active sites of adsorbent [42]. Fig. 7 shows the effect of initial pollutant concentrations (0.5–3.0 mg/l) on adsorption by the T-MC. As illustrated, the adsorption capacity increased by increasing the concentration of the adsorbate. Furthermore, Y. Salameh et al. explained that the amount of adsorption capacity onto charred dolomite increased with increasing the concentration of As(III,V) to 2 mg/l and finally reached a saturation point [18].

3.2.5. Effect of adsorbent dose

The amounts of a surfactant is considered as a basic variable in the adsorption studies as it determines the capacity of the adsorbent for a given initial content of As(III) solution. By monitoring the amount of surfactant, it is possible to study the impacts of an adsorption process in order to reach a maximum adsorption capacity of the adsorbent. The effect of the adsorbent dose on As(III) removal has been presented in Fig. 8, indicating that the removal efficiency increased with raising the adsorbent amount. The maximum removal of As(III) happened at the adsorbent dose of 1 g/L. Albadarin et al. reported similar results of Cr(IV) adsorption by dolomite; they suggested that, while the initial Cr(VI) concentration

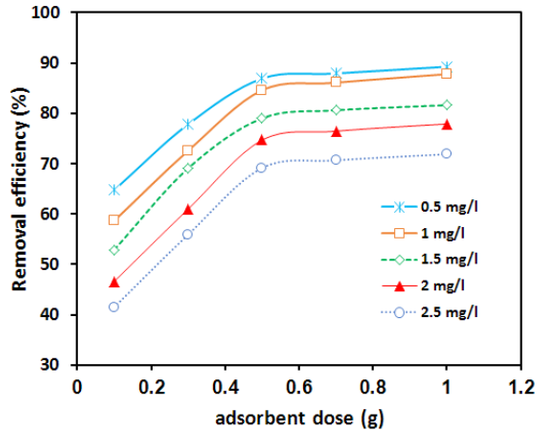

Fig. 8. Effect of adsorbent dose on As(III) adsorption onto T-MC: As(III) concentrations 0.5–3 mg/L, initial pH 6.0 and contact time 300 min.

was fixed, Cr(VI) ions could occupy just a certain amount of active sites. Therefore, an additional raise in the number of the active sites of dolomite does not influence the total Cr(VI) ions adsorbed. In general, it should be noted that, for each ion content, there is a corresponding adsorbent dose, at which adsorption equilibrium will be established [43].

3.3. Adsorption kinetics

Chemical reaction, diffusion and mass transfer are the main controlling mechanisms of adsorption processes. On the whole, kinetic models are employed to test experimental data of As(III) adsorption. In order to select optimum operating conditions for the full-scale batch process, the kinetics of As(III) adsorption onto T-MC is thus essential. The kinetic parameters, which are beneficial for the prediction of adsorption rate, present basic information for designing and modeling the adsorption processes. Therefore, the

kinetics of As(III) adsorption onto T-MC was analyzed by means of the pseudo-first-order, pseudo-second-order, Elovich and intra particle diffusion kinetic models [44]. The conformity between the experimental data and the model predicted values was explained by the correlation coefficients (R^2, values close or equal to 1). The relatively higher value is the more applicable model to the kinetics of As(III) adsorption onto the adsorbent.

3.3.1 Pseudo-first-order kinetic model

The pseudo-first-order kinetic model [45] assumes that the change rates of solute uptake with time is directly proportional to difference in saturation concentration and the amount of solid uptake with time. In most cases, the adsorption reaction is preceded by diffusion through a boundary, the kinetics following the pseudo-first-order rate equation. The rate constant of adsorption is explained as a first-order rate expression by the following equation:

$$\frac{dq_t}{dt} = k_1(q_e - q_t) \tag{4}$$

where q_e and q_t are the amounts of metal ion adsorbed (mg g^{-1}) at contact time t (min) and at equilibrium, respectively, and k_1 is the pseudo-first-order rate constant (min^{-1}). After integrating and rearranging Eq. (4), the rate law for a pseudo-first-order reaction becomes as follows [45]:

$$\log(q_e - q_t) = \log q_e - \frac{k_1}{2.303}t \tag{5}$$

The plot log ($q_e - q_t$) vs. t should give a straight line with slope of $-(k_1/2.303)$ and intercept log q_e which allows the calculation of adsorption rate constant k_1 and equilibrium adsorption capacity. It may be seen that the experimental data point does not fit a straight line. Table 2 gives a breakdown of the calculated values of respective parameters of the first order kinetic model. From the values (experimental and calculated) in Table 2, it may be concluded that the kinetics of As(III) adsorption on T-MC does not follow the pseudo first order kinetic model.

3.3.2. Pseudo-second-order kinetic model

The adsorption process with chemisorptions being the rate-control follows the pseudo second-order model [52, 53]. The sorption kinetics may be represented by the pseudo-second-order model as follows:

$$\frac{dq_t}{dt} = k_2(q_e - q_t)^2 \tag{6}$$

where k_2 is the equilibrium rate constant for pseudo-second-order sorption (g (mg min)$^{-1}$). Integrating Eq. (6) and rearranging the rate law for a pseudo-second -order reaction becomes as follows:

$$\frac{t}{q_t} = \frac{1}{k_2 q_e^2} + \frac{t}{q_e} \tag{7}$$

the plot of t/q_t vs. t gives a straight line with slope of $1/q_e$ and intercept of $1/(k_2 q_e^2)$ and these parameters were calculated from the slope, the value of k_2 is determined from the intercept and their values in addition to corresponding regression coefficients (R^2 = 0.9999) values are shown in Table 2. From the values of regression coefficients (close to unity), it is confirmed that the sorption kinetics of As(III) follows a pseudo second order process. It may also be found that the calculated values are very close to those of experimentally obtained data. Therefore, it may be concluded that the As(III) adsorption on the T-MC fits better the pseudo-second-order kinetic model than that the first-order kinetic model and the process is chemisorptions controlled. Ali Kara et al. reported similar results of of Cr(VI) on the m-poly(EG-VPBA) micro particles [46]. The second-order

Table 2
Kinetic parameters of As(III) adsorption onto T-MC under the following conditions: 0.5 g adsorbent over 0.5–3.0 mg/L, 5–300 min contact time at optimum conditions of other variables

Parameter values: Concentration As(III) (ppm)							
Models	Parameters	0.5	1.0	1.5	2.0	2.5	3.0
First order kinetic model:	K_1	0.179	0.168	0.164	0.162	0.161	0.150
Log $(q_e - q_t) = \log(q_e) - (K_1/2.303)t$	q_e (cal)	10.38	19.14	34.40	44.38	91.64	170.37
	R^2	0.9761	0.9203	0.9122	0.9602	0.8784	0.8419
Second order kinetic model:	K_2	1.38	0.576	0.339	0.236	0.195	0.092
$t/q_t = 1/k_2 q_e^2 + (1/q_e)t$	q_e (cal)	0.088	0.172	0.244	0.309	0.355	0.414
	R^2	0.9990	0.9988	0.9987	0.9990	0.9986	0.9983
	h	0.724	1.735	2.95	4.24	5.13	10.81
Intraparticle diffusion	K_{dif}	0.0021	0.0047	0.0075	0.0107	0.0128	0.0188
$q_t = K_{id} t^{1/2} + C$	C	0.0531	0.0943	0.1194	0.1316	0.1446	0.1917
	R^2	0.9014	0.9288	0.9431	0.9155	0.8794	0.9133
Elovich	β	0.18	0.11	0.09	0.05	0.03	0.02
$q_t = 1/\beta \ln(\alpha\beta) + 1/\beta \ln(t)$	R^2			0.9821	0.9843		0.9828
Experimental date	q_e (exp)			0.24			0.40

rate constants were applied to calculate the initial sorption rate (h), given by Eq. (8) (Table 2).

$$h = k_2 q_e^2 \quad (8)$$

3.3.3. Elovich equation

In this model with known Eq. (9):

$$q_t = 1/\beta \ln(\alpha\beta) + 1/\beta \ln (t) \quad (9)$$

where α is the initial adsorption rate (mg (g min)$^{-1}$) and β is the desorption constant related to the extent of surface coverage and activation energy for chemisorption (g mg^{-1}). The parameters (1/β) and (1/β)ln(αβ) can be calculated from the slope and intercept of the linear plot of q_t vs. ln(t). The attained R^2 value of this model was <0.9875 for As(III) initial concentration in the range of 0.5–3 mg L^{-1} on T-MC adsorbent (Table 2). The parameter 1/β is related to the number of sites available for adsorption while (1/β)ln(αβ) is the adsorption quantity when ln t is zero. Adsorption quantity at 10 min is helpful in understanding the adsorption behavior of the first step [47].

3.3.4. Intra-particle diffusion model

In the intra-particle diffusion model [48,49], it is assumed that the mechanism for the metal ion (As) removal by adsorption on a sorbent material occurs via four steps: a) migration of metal ion from bulk solution to the surface of the adsorbent by bulk diffusion, b) diffusion of metal ion by the boundary layer to the surface of the adsorbent via film diffusion; c) the transport of the metal ion from the surface to the interior pores of the particle occur through intra-particle-diffusion or pore diffusion mechanism and d) the adsorption of metal ion at an active site on the surface of material by chemical reaction through ion-exchange, complexation and/or chelation. On the whole, both the liquid phase mass transport rate and intra-particle mass transport rate control the As(III) sorption. So as to tackle either the particle size or particle shape, pore-diffusion models should be formulated. The adsorption is a diffusive mass transfer process, which its rate can be stated in terms of the square root of time (t). The intra-particle-diffusion model is described as follows [50,51]:

$$q_t = k_1 t^{0.5} \quad (10)$$

where q_t is the fraction As(III) uptake (mg g^{-1}) at time t, k_i is the intra-particle-diffusion rate constant (mg g^{-1} min^{-1}) and C is the intercept (mg g^{-1}). The plot of q_t vs. $t^{0.5}$ gives k_i as slope and C as intercept. The intercept represents the impact of the thickness of the boundary layer. Minimum is the intercept length, adsorption is less boundary layer controlled. Table 2 shows both the values of k_i and C and regression constant (R^2). The straight line is gained signifying that the metal ions are transported to the external surface of the adsorbent via film diffusion and its rate is very quick. As a result, the adsorption of As(III) on T-MC is a complicated process and either intraparticle diffusion or surface sorption (film diffusion) are effective in the rate-limiting step. Also, it should be noted that the intraparticle diffusion is not the only rate limiting mechanism as the line does not pass via the origin.

3.4. Adsorption isotherms

So as to study the adsorption capacity and the characteristics of adsorption, the adsorption isotherm plays a basic role. In this research, in order to analyze adsorption As(III), the Langmuir, Freundlich and Dubinin-Radushkevich (D-R) isotherms models were employed [44,48]. The adsorption mechanism and maximum adsorption capacity on the adsorbent surface can be described by the Langmuir and Frundlich adsorption isotherms.

3.4.1. Langmuir adsorption isotherm model

The well-known linear form of Langmuir's adsorption isotherm equation [Eq. (11)] was applied for the As(III)–T-MC system.

$$C_e/q_e = 1/K_a Q_m + C_e/Q_m \quad (11)$$

where q_e is the number of moles of solute adsorbed per unit weight at concentration C (mol g^{-1}), C_e is the equilibrium molar concentration of As(III) (mol L^{-1}), Q_m is the maximum adsorption capacity and K_a is the energy of adsorption. At all temperatures, the $1/C_e$ vs. $1/q_e$ graphs gives straight lines with appreciable values of the regression coefficient (R^2) close to unity, verifying the Langmuir adsorption model and ascertaining that monolayer formation happens over the adsorption of As(III) on the surface of T-MC. On the basis of gradient and interception of these straight lines, Langmuir constant 'K_a' and number of moles of the metal ions adsorbed per unit weight of the adsorbent (Q_m) were evaluated and the results have been shown in Table 3. The correlation coefficients and high maximum monolayer capacity (1.48–0.25 mg g^{-1} using 0.1–1.0 g adsorbent) illustrate strong positive evidence on the fitness of equilibrium data of As(III) adsorption by the Langmuir model (Table 3). To confirm this result, the favorable or unfavorable As(III) adsorption onto the Langmuir model was judged by calculation of the separation factor (R_L) as follows [48,51]:

$$R_L = 1/(1+K_a C_0) \quad (12)$$

where k_a (L mg^{-1}) is the Langmuir constant and C_0 (mg L^{-1}) is the initial concentration. The adsorption process is considered as favorable when the R_L value lies between 0 and 1. In this study, the R_L value was found to be lower than 1, suggesting the favorable adsorption and good fitness of the Langmuir model to explain experimental data. On the other hand, a rise in R_L value with increasing initial metal ion content and adsorbent dose caused As(III) adsorption onto T-MC to rise.

3.4.2. The Freundlich isotherm

The Freundlich isotherm (nonlinear model) could describe the exponential adsorption of target compound on heterogeneous surfaces [50]. The Freundlich isotherm Eq. (13) can be simplified to the following equation:

$$\ln q_e = \ln K_F + (1/n)\ln C_e \quad (13)$$

where constants such as K_f showing information on the bonding energy and known as the adsorption or distribution coefficient and represents the quantity of As(III) adsorbed onto the adsorbent. $1/n$ presents the adsorption intensity of As(III) onto the adsorbent (surface heterogeneity). The value closer to zero by rising heterogeneous nature of surface ($1/n < 1$) is indicative of a normal Langmuir isotherm while $1/n$ above 1 shows bi-mechanism and cooperative adsorption. The applicability of the Freundlich adsorption isotherm was evaluated by plotting $\ln(q_e)$ vs. $\ln(C_e)$ and respective values for this model constants at various amounts of adsorbent are given in Table 3. The correlation coefficients ($R^2 = 0.9768$) of this model depicts that the Freundlich model has lower efficiency compare to the Langmuir model.

3.4.3. The Temkin isotherm

The R^2 value indicates the appropriateness of models for the representation of method applicability for description of experimental data. Although the Langmuir and even Freundlich models have reasonable and an acceptable R^2 value, the applicability of other models like Temkin isotherm has commonly been used in the following linear form [50,56,59]: the Temkin isotherm [Eq. (14)] can be simplified to the following equation:

$$q_e = B_1 \ln K_T + B_1 \ln C_e \quad (14)$$

where $B_1 = (RT)/b$ is related to the heat of adsorption, T is the absolute temperature in Kelvin and R is the universal gas constant, 8.314 (J mol^{-1} K^{-1}) [48, 52]. The adsorption data were analyzed based on the linear form of the Temkin isotherm. It was found that the Temkin isotherm is effectively applicable for fitting the As(III) adsorption onto T-MC. Table 3 gives the linear isotherm constants and coefficients. When there was a rise in the dosage of T-MC (0.1 to 1.0 g), the heat of As(III) adsorption onto T-MC increased from 0.384 to 0.057 kJ mol^{-1}. The correlation coefficient ($R^2 = 0.9870$) attained from the Temkin model was comparable to those for the Langmuir model; this illustrates the less applicability of Temkin model to the adsorption of As(III) onto T-MC.

3.4.4. D–R adsorption isotherm model

So as to describe the nature of the evolving adsorption process, the D–R adsorption isotherm model was utilized [53,54]:

$$\ln q_e = \ln Q_s - B\varepsilon^2 \quad (15)$$

where q_e is the amount of As(III) adsorbed per unit weight of the adsorbent (mg g^{-1}), Q_s is the maximum sorption capacity provided by the intercept (μmol g^{-1}), B (mol^2 J^{-2}) is the activity coefficient related to mean sorption energy, and ε [Eq. (16)] is Polanyi potential [53,55].

$$\varepsilon = RT \ln(1 + 1/C_e) \quad (16)$$

where R is universal gas constant and T is temperature in Kelvin. The activity coefficient (B) and the adsorption capacities ($\ln Q_s$) were investigated from the slopes and intercepts of the plot $\ln q_e$ vs. ε^2 at 25°C; Table 3 indicates the results. The mean sorption energy (E) was calculated from the values of β by the following equation [44,55]:

$$E = 1/\sqrt{2B} \quad (17)$$

On the basis of the values of B, gained from the D–R isotherm graph, the values of mean sorption energy were calculated at each temperature. The calculated value of constant of the

Table 3
Isotherm constants of As(III) adsorption onto T-MC at 0.5–3 mg L^{-1} of initial As(III) concentration, pH = 6, 300 min contact time and room temperature

Adsorbent (g)						
Isotherm & Equation	Parameters	0.1	0.3	0.5	0.7	1.0
Langmuir	Q_m (mg g^{-1})	1.48	0.63	0.50	0.36	0.25
$C_e/q_e = 1/K_aQ_m + C_e/Q_m$	K_a (L mg^{-1})	1.61	2.42	3.09	3.35	3.90
	R_L	0.17-0.55	0.12-0.45	0.10-0.39	0.09-0.37	0.08-0.34
	R^2	0.9999	0.9975	0.9964	0.9956	0.9949
Freundlich	$1/n$	0.527	0.525	0.519	0.509	0.504
$\ln q_e = \ln K_F + (1/n)\ln C_e$	K_F (L mg^{-1})	0.87	0.44	0.41	0.31	0.22
	R^2	0.9729	0.9596	0.9768	0.9738	0.9696
Tempkin	B_1	0.384	0.163	0.115	0.082	0.057
$q_e = B_1 \ln K_T + B_1 \ln C_e$	K_T (L mg^{-1})	11.85	17.77	29.07	32.63	37.50
	R^2	0.9679	0.9757	0.9803	0.9870	0.9827
Dubinin and Radushkevich	Q_s (mg g^{-1})	1.10	0.50	0.39	0.29	0.20
$\ln q_e = \ln Q_s - B\varepsilon^2$	B	5E-08	4E-08	3E-08	3E-08	3E-08
	E (J/mol) = $1/(2B)^{1/2}$	3162.28	3535.53	4082.5	4082.5	4082.5
	R^2	0.9806	0.9860	0.9871	0.9889	0.9885

D–R model stated that the saturation adsorption capacity ranged from 1.10 to 0.20 (mg g^{-1}) for T-MC, which is consistent with the respective Langmuir value. The values of E were between 3162.28 and 4082.5 J mol^{-1} for T-MC. It proves that the physico-sorption process plays a basic role in the adsorption of As(III). The positive correlation between E and mass of adsorbent shows a higher tendency of metal ion (As) for adsorption onto the adsorbents surface.

3.4.4.1. Comparison of adsorption capacity with various adsorbents

A comparative study is indicated in Table 4 for As(III) removal via different adsorbents stated in literature. The adsorption capacity changes and depends mainly on the initial As(III) concentration and characteristics of the individual adsorbent. Apparently, our results are similar to the investigation with similar initial concentrations.

3.5. Effects of temperature

Changing temperature will change the equilibrium capacity of the adsorbent for a particular adsorbate [56]. Thermodynamic parameters represent valuable information about the adsorption nature. The endothermic or exothermic nature of the adsorption process was determined by conducting similar experiments at various temperatures in ranging from 288–318 K. The following equations (18)–(20) have been applied to evaluate the thermodynamic constants including Gibbs free energy (ΔG°), enthalpy (ΔH) and entropy (ΔS) [57].

$$\Delta G^\circ = -RT \ln K_c \quad (18)$$

$$\Delta G^\circ = \Delta H - T\Delta S \quad (19)$$

$$\ln K_c = \Delta S/R - \Delta H/RT \quad (20)$$

where R is the universal gas constant, T is the absolute temperature (K) and K_c is the thermodynamic equilibrium constant (acquired from Langmuir model) be calculated from the relation C_e/q_e vs. C_e at different temperatures and extrapolating to zero. The entropy (J/k mol) and enthalpy (kJ/mol) of the adsorption were obtained from the intercept and slope of plot of ln K_c vs. 1/T, respectively (Fig. 9).

The values of thermodynamic parameters are shown in Table 5.

As can be seen, the Gibbs free energy values for the adsorption in the range of temperatures were positive in low temperatures and negative in high temperatures. A decrease in ΔG° values with an increase in temperature confirms the feasibility of the process and spontaneous nature of the adsorption of As(III) onto T-MC. The positive value of ΔH suggests the endothermic nature of adsorption, while the positive value of ΔS indicates an increase in randomness at the solid/solution interface following adsorption.

In order to claim that the physical adsorption is the predominant mechanism, the values of activation energy (E_a) and sticking probability (S^*) were estimated from the experimental data using modified Arrhenius type equation according to surface coverage (θ) is as follows[58]:

$$S^* = (1-\theta)e^{E_a/RT} \quad (21)$$

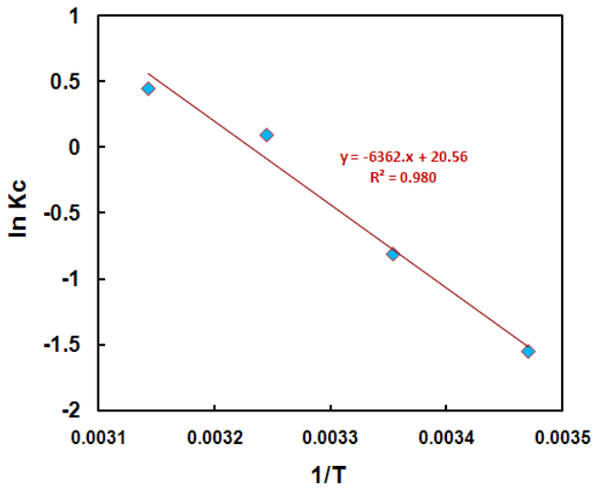

Fig. 9. plot of ln K_c versus 1/T for As(III) adsorption onto T-MC.

Table 4
Comparison of adsorption capacities of the adsorbents

Adsorbents	Concentration (mg L^{-1})	Adsorption capacity (mg g^{-1})	Best fit isotherm	Ref.
Shale sedimentary rock	0.1–1	0.987	Langmuir	[58]
Charred dolomite	0.05–2	1.846	Freundlich	[18]
Natural siderite	0.25–2	0.104	Langmuir Freundlich	[60]
Chitosan-Fe-crosslinked complex	5–50	13.4	Langmuir- Freundlich	[15]
zirconium polyacrylamide	10–100	41.48	Langmuir	[14]
iron-modified activated carbon	20–22	38.8	Langmuir	[61]
iron oxide coated sand	0.1–1	0.028	Langmuir	[62]
T-MC	0.5–3	1.48	Langmuir	This study

Table 5
Thermodynamic parameters for adsorption of As(III) onto 0.1 g L^{-1} T-MC at pH = 6 atinitial As(III) concentrations of 1.5 mg L^{-1}

Parameter	Temperature(K)				
	288.15	298.15	308.15	318.15	
K_c	0.211	0.443	1.1	1.56	
ΔG° (kJ/mol)	3.62	1.91	0.2	–1.5	
	ΔS° (J/molK)	ΔH° (kJ/mol)		Ea (kJ/mol)	S
	170.95	52.9		44.49	29×10^{-10}

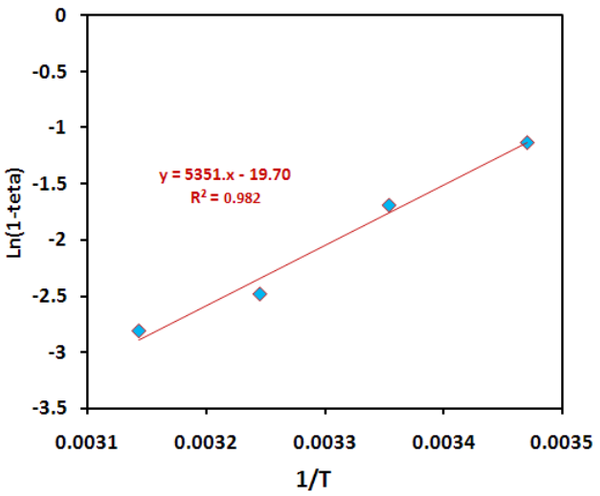

Fig. 10. plot of ln(1 − θ) versus 1/T for As(III) adsorption onto T-MC.

The parameter S^* indicates the measure of the potential of an adsorbate to remain on the adsorbent indefinite. The value of sticking probability lies in the range $0< S^*<1$ which depends on the temperature of the system. As seen from Table 4, the S^* value of As(III) adsorption by T-MC is in range of $0 < S^*< 1$.

The surface coverage (θ) is obtained from Eq. (22).

$$\theta = 1- C_e/C_0 \quad (22)$$

E_a and S^* are taken from a plot of ln(1 − θ) vs. 1/T (Fig. 10).

4. Conclusion

It can be said that montmorillonite modified with the surfactant can be introduced as a suitable, green and low-cost adsorbent with high removal efficiency around 94% for As(III). In this research, the maximum adsorption rate of As(III) on T-MC was achieved with the surfactant loading rate of 70% CEC, contact time of 5 h, pH of 6 and temperature of 45°C. The Langmuir isotherm gave a better fit to adsorption isotherms than the Freundlich isotherm by means of the linear method; Langmuir was the best model for fitting the experimental data that may be related to the high Langmuir surface area of the adsorbent. The kinetic study of As(III) on T-MC was conducted according to the pseudo-first order, pseudo-second-order, Elovich and intra-particle diffusion equations. The data illustrated that the adsorption kinetics followed the pseudo-second-order rate. Thermodynamic study indicated that the uptake of As(III) by T-MC was spontaneous, endothermic and favorable at high temperature. The present adsorbent may be considered as an alternative adsorbent for a better performance of As(III) removal from aqueous medium.

Acknowledgements

The authors would gratefully thank Ilam University of Medical Sciences for supporting us with equipment and experiments.

References

[1] S.K.R. Yadanaparthi, D. Graybill, R. von Wandruszka, Adsorbents for the removal of arsenic, cadmium, and lead from contaminated waters, J. Hazard. Mater., 171 (2009) 1–15.
[2] J. Tong, H. Guo, C. Wei, Arsenic contamination of the soil–wheat system irrigated with high arsenic groundwater in the Hetao Basin, Inner Mongolia, China, Sci. Total Environ., 496 (2014) 479–487.
[3] X.-J. Gong, W.-G. Li, D.-Y. Zhang, W.-B. Fan, X.-R. Zhang, Adsorption of arsenic from micro-polluted water by an innovative coal-based mesoporous activated carbon in the presence of co-existing ions, Int. Biodeter. Biodegr., 102 (2015) 256–264.
[4] Y. Wang, J. Duan, S. Liu, W. Li, J. van Leeuwen, D. Mulcahy, Removal of As(III) and As (V) by ferric salts coagulation–Implications of particle size and zeta potential of precipitates, Sep. Purif. Technol., 135 (2014) 64–71.
[5] S. Xia, S. Shen, X. Xu, J. Liang, L. Zhou, Arsenic removal from groundwater by acclimated sludge under autohydrogenotrophic conditions, J. Environ. Sci., 26 (2014) 248–255.
[6] C.O. Cope, D.S. Webster, D.A. Sabatini, Arsenate adsorption onto iron oxide amended rice husk char, Sci. Total Environ., 488 (2014) 554–561.
[7] A. Maiti, B.K. Thakur, J.K. Basu, S. De, Comparison of treated laterite as arsenic adsorbent from different locations and performance of best filter under field conditions, J. Hazard. Mater., 262 (2013) 1176–1186.
[8] N.B. Issa, V.N. Rajaković-Ognjanović, A.D. Marinković, L.V. Rajaković, Separation and determination of arsenic species in water by selective exchange and hybrid resins, Anal. Chim. Acta, 706 (2011) 191–198.
[9] D. Lakshmanan, D. Clifford, G. Samanta, Arsenic removal by coagulation with aluminum, iron, titanium, and zirconium, American Water Works Association, 100 (2008) 76.
[10] S. Su, X. Zeng, L. Bai, L. Li, R. Duan, Arsenic biotransformation by arsenic-resistant fungi Trichoderma asperellum SM-12F1, Penicillium janthinellum SM-12F4, and Fusarium oxysporum CZ-8F1, Sci. Total Environ., 409 (2011) 5057–5062.
[11] M.C.S. Faria, R.S. Rosemberg, C.A. Bomfeti, D.S. Monteiro, F. Barbosa, L.C.A. Oliveira, M. Rodriguez, M.C. Pereira, J.L. Rodrigues, Arsenic removal from contaminated water by ultrafine δ-FeOOH adsorbents, Chem. Eng. J., 237 (2014) 47–54.
[12] A. Yürüm, Z.Ö. Kocabaş-Ataklı, M. Sezen, R. Semiat, Y. Yürüm, Fast deposition of porous iron oxide on activated carbon by microwave heating and arsenic (V) removal from water, Chem. Eng. J., 242 (2014) 321–332.

[13] T.S. Singh, K. Pant, Equilibrium, kinetics and thermodynamic studies for adsorption of As(III) on activated alumina, Sep. Purif. Technol., 36 (2004) 139–147.
[14] S. Mandal, M.K. Sahu, R.K. Patel, Adsorption studies of arsenic (III) removal from water by zirconium polyacrylamide hybrid material (ZrPACM-43), Water Res. Ind., 4 (2013) 51–67.
[15] H.H. dos Santos, C.A. Demarchi, C.A. Rodrigues, J.M. Greneche, N. Nedelko, A. Ślawska-Waniewska, Adsorption of As(III) on chitosan-Fe-crosslinked complex (Ch-Fe), Chemosphere, 82 (2011) 278–283.
[16] J. Giménez, M. Martínez, J. de Pablo, M. Rovira, L. Duro, Arsenic sorption onto natural hematite, magnetite, and goethite, J. Hazard. Mater., 141 (2007) 575–580.
[17] S. Kango, R. Kumar, Low-cost magnetic adsorbent for As(III) removal from water: adsorption kinetics and isotherms, Environ. Monit. Assess., 188 (2016) 60.
[18] Y. Salameh, A.B. Albadarin, S. Allen, G. Walker, M.N.M. Ahmad, Arsenic(III,V) adsorption onto charred dolomite: Charring optimization and batch studies, Chem. Eng. J., 259 (2015) 663–671.
[19] M. Rahim, M.R.H.M. Haris, Application of biopolymer composites in arsenic removal from aqueous medium: A review: Arsenic removal from aqueous medium using polymeric biocomposites, J. Radiat. Res. Appl. Sci., 8 (2015) 255–263.
[20] M.L. Chávez, L. de Pablo, T.A. García, Adsorption of Ba2+ by Ca-exchange clinoptilolite tuff and montmorillonite clay, J. Hazard. Mater., 175 (2010) 216–223.
[21] K.G. Bhattacharyya, S.S. Gupta, Adsorption of a few heavy metals on natural and modified kaolinite and montmorillonite: A review, Adv. Colloid Interfac., 140 (2008) 114–131.
[22] S.-H. Lin, R.-S. Juang, Heavy metal removal from water by sorption using surfactant-modified montmorillonite, J. Hazard. Mater., 92 (2002) 315–326.
[23] Q. Feng, Z. Zhang, Y. Chen, L. Liu, Z. Zhang, C. Chen, Adsorption and Desorption Characteristics of Arsenic on Soils: Kinetics, Equilibrium, and Effect of Fe (OH) 3 Colloid, H 2 SiO 3 Colloid and Phosphate, Procedia Environ. Sci., 18 (2013) 26-36.
[24] Z. Sun, Y. Park, S. Zheng, G.A. Ayoko, R.L. Frost, XRD, TEM, and thermal analysis of Arizona Ca-montmorillonites modified with didodecyldimethylammonium bromide, J. Colloid Interfac., 408 (2013) 75–81.
[25] L. Wang, A. Wang, Adsorption properties of Congo Red from aqueous solution onto surfactant-modified montmorillonite, J. Hazard. Mater., 160 (2008) 173–180.
[26] J. Su, H.-G. Huang, X.-Y. Jin, X.-Q. Lu, Z.-L. Chen, Synthesis, characterization and kinetic of a surfactant-modified bentonite used to remove As(III) and As (V) from aqueous solution, J. Hazard. Mater., 185 (2011) 63–70.
[27] D. Chen, J. Chen, X. Luan, H. Ji, Z. Xia, Characterization of anion–cationic surfactants modified montmorillonite and its application for the removal of methyl orange, Chem. Eng. J., 171 (2011) 1150–1158.
[28] A. Maiti, J.K. Basu, S. De, Experimental and kinetic modeling of As(V) and As(III) adsorption on treated laterite using synthetic and contaminated groundwater: Effects of phosphate, silicate and carbonate ions, Chem. Eng. J., 191 (2012) 1–12.
[29] X. Ren, Z. Zhang, H. Luo, B. Hu, Z. Dang, C. Yang, L. Li, Adsorption of arsenic on modified montmorillonite, Appl. Clay Sci., 97–98 (2014) 17–23.
[30] K.G. Bhattacharyya, S.S. Gupta, Kaolinite, montmorillonite, and their modified derivatives as adsorbents for removal of Cu (II) from aqueous solution, Sep. Purif. Technol., 50 (2006) 388–397.
[31] X. Song, S. Wang, L. Chen, M. Zhang, Y. Dong, Effect of pH, ionic strength and temperature on the sorption of radionickel on Na-montmorillonite, Appl. Radiat. Isotopes, 67 (2009) 1007–1012.
[32] M. Sharafimasooleh, S. Bazgir, M. Tamizifar, A. Nemati, Adsorption of hydrocarbons on modified nanoclays, in: IOP Conference Series: Materials Science and Engineering, IOP Publishing, 2011, pp. 182012.
[33] L.M. Camacho, R.R. Parra, S. Deng, Arsenic removal from groundwater by MnO2-modified natural clinoptilolite zeolite: Effects of pH and initial feed concentration, J. Hazard. Mater., 189 (2011) 286–293.
[34] W. Luo, K. Sasaki, T. Hirajima, Surfactant-modified montmorillonite by benzyloctadecyldimethylammonium chloride for removal of perchlorate, Colloid. Surface. A., 481 (2015) 616–625.
[35] D. Bhardwaj, M. Sharma, P. Sharma, R. Tomar, Synthesis and surfactant modification of clinoptilolite and montmorillonite for the removal of nitrate and preparation of slow release nitrogen fertilizer, J. Hazard. Mater., 227–228 (2012) 292–300.
[36] M. Ghaedi, A. Ansari, M. Habibi, A. Asghari, Removal of malachite green from aqueous solution by zinc oxide nanoparticle loaded on activated carbon: kinetics and isotherm study, J. Ind. Eng. Chem., 20 (2014) 17–28.
[37] J.-Q. Jiang, C. Cooper, S. Ouki, Comparison of modified montmorillonite adsorbents: part I: preparation, characterization and phenol adsorption, Chemosphere, 47 (2002) 711–716.
[38] M. Hamayun, T. Mahmood, A. Naeem, M. Muska, S.U. Din, M. Waseem, Equilibrium and kinetics studies of arsenate adsorption by FePO4, Chemosphere, 99 (2014) 207–215.
[39] X. Dou, D. Mohan, C.U. Pittman Jr, Arsenate adsorption on three types of granular schwertmannite, Water Res., 47 (2013) 2938–2948.
[40] V. Zaspalis, A. Pagana, S. Sklari, Arsenic removal from contaminated water by iron oxide sorbents and porous ceramic membranes, Desalination, 217 (2007) 167–180.
[41] X. Sun, C. Hu, J. Qu, Preparation and evaluation of Zr-β-FeOOH for efficient arsenic removal, J. Environ. Sci., 25 (2013) 815–822.
[42] P. Mondal, C.B. Majumder, B. Mohanty, Effects of adsorbent dose, its particle size and initial arsenic concentration on the removal of arsenic, iron and manganese from simulated ground water by Fe3+ impregnated activated carbon, J. Hazard. Mater., 150 (2008) 695–702.
[43] A.B. Albadarin, C. Mangwandi, A.a.H. Al-Muhtaseb, G.M. Walker, S.J. Allen, M.N.M. Ahmad, Kinetic and thermodynamics of chromium ions adsorption onto low-cost dolomite adsorbent, Chem. Eng. J., 179 (2012) 193–202.
[44] K. Ahmadi, M. Ghaedi, A. Ansari, Comparison of nickel doped Zinc Sulfide and/or palladium nanoparticle loaded on activated carbon as efficient adsorbents for kinetic and equilibrium study of removal of Congo Red dye, Spectrochim. Acta A., 136 (2015) 1441–1449.
[45] S. Lagergren, Zur theorie der sogenannten absorption gelöster stoffe, PA Norstedt & söner, 1898.
[46] A. Kara, E. Demirbel, N .Tekin,B. Osman, N. Beşirli, Magnetic vinylphenyl boronic acid microparticles for Cr(VI) adsorption: kinetic, isotherm and thermodynamic studies, , J. Hazard. Mater., 286, (2015) 612–623.
[47] Y.-S. Ho, G. McKay, Pseudo-second order model for sorption processes, Process Biochem., 34 (1999) 451–465.
[48] M. Ghaedi, A. Ansari, F. Bahari, A. Ghaedi, A. Vafaei, A hybrid artificial neural network and particle swarm optimization for prediction of removal of hazardous dye brilliant green from aqueous solution using zinc sulfide nanoparticle loaded on activated carbon, Spectrochim. Acta A., 137 (2015) 1004–1015.
[49] W. Weber, J.C. Morris, Equilibria and capacities for adsorption on carbon, Sanitary Eng. Div, 90 (1964) 79–91.
[50] H. Freundlich, Uber die adsorption in losungen [Adsorption in solution]" Zeits. Phy. Chem., 57, (1906).
[51] I. Langmuir, The constitution and fundamental properties of solids and liquids. Part I. Solids, J. Am. Chem. Soc., 38 (1916) 2221–2295.
[52] M. Temkin, V. Pyzhev, Recent Modifications to Langmuir Isotherms, 1940.
[53] M. Dubinin, The potential theory of adsorption of gases and vapors for adsorbents with energetically nonuniform surfaces, Chem. Rev., 60 (1960) 235–241.
[54] M. Dubinin, Modern state of the theory of gas and vapour adsorption by microporous adsorbents, Pure Appl. Chem., 10 (1965) 309–322.

[55] L. Radushkevich, Potential theory of sorption and structure of carbons, Zh. Fiz. Khim., 23 (1949) 1410–1420.
[56] S. Wang, Y. Boyjoo, A. Choueib, Z. Zhu, Removal of dyes from aqueous solution using fly ash and red mud, Water Res., 39 (2005) 129–138.
[57] A. Kara, A. Tuncel, Kinetics, Isotherms and Thermodynamics of the Adsorption of Lead (II) Ions onto Porous Monosized Microspheres Possessing Imidazole Functional Groups, Adsorpt. Sci. & Technol, 29 (2011) 259–275.
[58] M. Ghaedi, F. Karimi, B. Barazesh, R. Sahraei, A. Daneshfar, Removal of Reactive Orange 12 from aqueous solutions by adsorption on tin sulfide nanoparticle loaded on activated carbon, J. Ind. Eng. Chem., 19 (2013) 756–763.
[59] N.Z. Yusof, M.A. Kassim, R. Ismail, A.R.M. Yusoff, Development of Simple and Cost Effective Method for Arsenic (III) Removal, Iranica J. Energy Environ., 5 (2009) 287–294.
[60] H. Guo, D. Stüben, Z. Berner, Adsorption of arsenic (III) and arsenic (V) from groundwater using natural siderite as the adsorbent, J. Colloid Interfac., 315 (2007) 47–53.
[61] W. Chen, R. Parette, J. Zou, F.S. Cannon, B.A. Dempsey, Arsenic removal by iron-modified activated carbon, Water Res., 41 (2007) 1851–1858.
[62] V. Gupta, V. Saini, N. Jain, Adsorption of As(III) from aqueous solutions by iron oxide-coated sand, J. colloid Interfac., 288 (2005) 55–60.